IEEE Robotics and Automation Letters (RA-L) paper, presented at ICRA 2026, Vienna, Austria. Cite as RA-L paper.

Entropy-Based Incremental Coverage Path Planning for Multi-UAV Persistent Monitoring

Cai Luo, *Senior Member, IEEE*, Lijun Wang, Jiucai Jin, Zhenpeng Du, and Wang Miao, *Member, IEEE*

***Abstract*—Oil spills continuously affect marine ecosystems and require rapid monitoring for effective emergency response. This letter tackles the problem of persistent monitoring for continuously changing and scattered oil spill regions through Entropy-Based Incremental Coverage Path Planning (EICPP). By using contour comparison between monitoring cycles, an incremental coverage mechanism is first introduced to focus on newly emerged oil spill regions. Then, a balanced region division algorithm is incorporated to handle scattered oil spill areas while ensuring equal workload distribution among UAVs. The entropy-based path planning enhances oil spill monitoring effectiveness by Drift Information Freshness (DIF) through prioritizing high-entropy regions under limited UAV resources. We evaluate the robustness and effectiveness of our method across multiple scenarios. Our method demonstrates clear advantages in DIF, achieving 19–25% improvements over strong baselines across different spill scales and about 19.6–24% on real-world oil spill datasets. It also substantially reduces total flight distance while consistently satisfying the 90% coverage requirement.**

***Index Terms*—Motion and path planning, environment monitoring and management, multi-robot systems.**

I. Introduction

OIL spills continuously impact marine ecosystems, coastal environments, and human activities [1], [2]. Therefore, monitoring of spilled oil is essential for emergency response, mitigation strategies, and environmental protection. However, existing monitoring approaches such as satellite remote sensing [3] and manual surveys exhibit limitations including constrained temporal-spatial resolution, limited efficiency, and reduced adaptability to rapidly changing conditions [4].

As a cost-effective moving platform, uncrewed aerial vehicles (UAVs) have demonstrated considerable potential in various applications, including environmental monitoring, emergency response, and search and rescue [5]. UAVs are becoming an effective tool for oil spill monitoring due to their flexibility, rapid deployment, and ability to collect high-resolution data in near real time [6]. Coverage Path Planning (CPP) is often applied to UAV monitoring since it can cover the entirety of a given Area Of Interest (AOI).

However, traditional CPP faces key challenges when dealing with oil spill area monitoring problems. Oil spill areas are constantly dynamic and irregularly shaped regions due to ocean currents, winds, and tides [7]. This makes traditional CPP methods [8] that are designed for static and regular polygonal regions ineffective. Specifically, traditional region partitioning methods such as Boustrophedon Cellular Decomposition (BCD) and Voronoi partitioning, when facing scattered and irregular oil spill areas, result in unbalanced region sizes and fail to maintain spatial continuity of partitioned regions. Additionally, due to the limited endurance of UAVs [9], [10], achieving high coverage rate while improving flight efficiency remains a critical challenge.

Meanwhile, most existing monitoring approaches [13] primarily focus on coverage completeness and operational efficiency, but often overlook the timeliness of the collected information. In dynamic scenarios such as oil spill monitoring, it is essential to maintain high information freshness, defined specifically as Drift Information Freshness (DIF), which refers to the extent to which the collected oil spill information reflects the latest state of the monitored environment. In the early stage of an oil spill, the slick undergoes rapid expansion and drift due to winds and currents. Timely and effective monitoring during this phase is critical for enabling rapid emergency response and containment actions [14]. Early intervention also helps to prevent the development of long-duration spills that pose more severe and persistent environmental risks [15]. Moreover, common response measures [16] (e.g., booms, skimmers, dispersants, bioremediation) all depend on up-to-date monitoring data, and delays can distort forecasts, miss containment opportunities, reduce effectiveness, and increase both response difficulty and economic losses. Therefore, the value of DIF lies in its ability to quantify the timeliness of monitoring data, ensuring that UAV-based systems provide information that maximally supports early-stage emergency response, thereby underscoring its practical significance.

To address these challenges, this letter proposes a multi-UAV monitoring framework for dynamic oil spill monitoring, as illustrated in Fig. 1. First, an incremental coverage mechanismis implemented to avoid rebundant monitoring of previously covered area. This mechanism focuses on newly emerged regions

Received 8 July 2025; accepted 2 November 2025. Date of publication 14 November 2025; date of current version 21 November 2025. This article was recommended for publication by Associate Editor X. Xiao and Editor A. Bera upon evaluation of the reviewers' comments. This work was supported in part by the National Key R&D Program of China under Grant 2021YFE0111600, in part by EU Horizon 2020 under Grant 101008297, in part by UKRI under Grant EP/Y036786/1, and in part by Horizon EU under Grant 101129910. *(Corresponding author: Lijun Wang.)*

Cai Luo and Lijun Wang are with the College of Oceanography and Space Informatics, China University of Petroleum (East China), Qingdao 266580, China (e-mail: tsai.lo.95@gmail.com; fmgg2026@gmail.com).

Jiucai Jin is with the First Institute of Oceanography, Ministry of Natural Resources, Qingdao 266580, China (e-mail: jinjiucai@fio.org.cn).

Zhenpeng Du and Wang Miao are with the Department of Computer Science, University of Exeter, EX4 4QF Exeter, U.K. (e-mail: duzhenpeng1997@gmail.com; wang.miao@exeter.ac.uk).

Digital Object Identifier 10.1109/LRA.2025.3632728

IEEE Robotics and Automation Letters (RA-L) paper, presented at ICRA 2026, Vienna, Austria. Cite as RA-L paper.

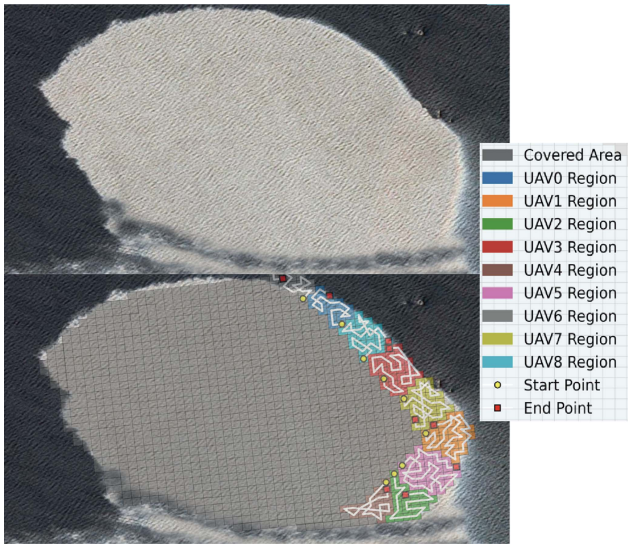

Fig. 1. The upper image shows a satellite observation of the Deepwater Horizon oil spill, with data obtained from [11], [12]. The lower image illustrates the coverage paths generated by the proposed method, based on a grid map constructed from the spill region, in which the newly emerged spill regions are partitioned into subregions (as indicated by the colored areas) and optimized using the DIF metric to produce the final coverage trajectories.

by comparing current and previous spill contours. Second, a balanced region division algorithm designed to handle irregular and scattered oil spill regions. It uses entropy-based clustering followed by iterative region balancing to ensure balanced workload distribution while maintaining spatial continuity. Finally, an information entropy-based model developed to ensure information freshness, enabling UAVs to prioritize the monitoring of the most critical dynamic change regions (i.e., high-entropy regions).

A. Related Work

Persistent monitoring is one of the important means to effectively collect key information in a region, such as atmospheric pollution [17] and wildfire. Ravi [18] proposed a proposed a meeting-based spatial scheduling approach that allows multiple agents to persistently monitor forest wildfires. Qing et al. [19] developed multi-UAV deployment strategies for persistent monitoring, focusing on different priorities for points of interest.

Coverage path planning [20] has become a fundamental strategy in muti-UAV persistent monitoring, ensuring that entire target areas are thoroughly scanned without leaving any gaps. For 2D fields, existing approaches are typically divided into decomposition-based methods and alternative strategies. Decomposition-based techniques first partition the workspace into manageable regions and then generate coverage paths for each region to achieve complete coverage [8].

According to the decomposition method adopted, these approaches can be further categorized into trapezoidal decomposition, boustrophedon decompositio, Morse-based cellular decomposition, and exact cell decomposition [8]. Other strategies are based on a grid representation of the area, including spanning tree coverage [21], and neural network-based approaches [22]. Some methods utilize exact cellular decomposition in combination with predefined coverage patterns, such as back-and-forth sweeping or spiral trajectories, to optimize path efficiency [23], [24]. In contrast, approximate cellular decomposition constructs a graph from the resulting cells and applies graph search algorithms to generate coverage paths [10]. However, most methods are designed for static monitoring scenarios and tend to be less effective in addressing changing areas in dynamic environments such as oil spills. When applied to such cases, they often result in redundant coverage and delayed monitoring of critical regions, ultimately reducing overall efficiency.

B. Contribution

The main contributions of this work are as follows:

1) We propose a novel incremental coverage path planning framework that integrates balanced region division with a jump-enabled, entropy-based strategy. By incorporating an incremental mechanism, the framework reduces redundant monitoring and improves robustness in handling highly fragmented oil spill regions.
2) We introduce a novel and meaningful metric, DIF, which explicitly quantifies the timeliness of monitoring information and has been overlooked in prior coverage path planning research.
3) We evaluate our framework (EICPP) on diverse spill monitoring scenarios, demonstrating the effectiveness of combining incremental coverage, entropy-based clustering for region division, and entropy-guided greedy path planning, thereby improving DIF and reducing flight distance.

The remainder of this letter is organized as follows. Section II presents the system model and formalizes the multi-UAV oil spill monitoring problem, including the dynamic oil spill model, grid-based representation, uncertainty modeling, and performance metrics. Section III introduces the proposed monitoring framework, including the incremental coverage mechanism, region division, and entropy-based path planning. Experiments setup and performance evaluation across multiple oil spill scenarios are provided in Section IV. Finally, Section V concludes the paper.

II. System Model and Problem Formulation

A. Oil Spill Dynamic Model and Grid Representation

Oil spill monitoring requires an accurate description of spill dynamics to enable effective response. In our approach, the OpenDrift software [25] is used as the core simulation tool, integrating physical oceanographic models with oil weathering processes, combined with real-world wind and ocean current data, to generate realistic spill trajectories. For a given monitoring area $A \subset \mathbb{R}^2$, we denote the oil concentration at position (x, y) and time t as $C(x, y, t)$. The continuous spill data produced by the simulation are then converted into a discrete grid representation suitable for UAV-based monitoring.

To facilitate UAV path planning, we transform the continuous concentration field into a discrete grid representation. The monitoring area is divided into an $n \times n$ grid G, where each

IEEE Robotics and Automation Letters (RA-L) paper, presented at ICRA 2026, Vienna, Austria. Cite as RA-L paper.

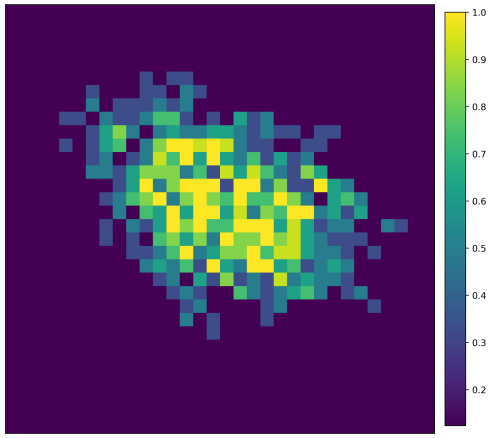

Fig. 2. The spatial entropy map is visualized as a heatmap.

cell $g_{i,j} \in G$ corresponds to a specific geographical area. The oil concentration for each grid cell is calculated by averaging the continuous concentration over the cell area, mathematically expressed as $c_{i,j}(t) = \frac{1}{|g_{i,j}|} \iint_{g_{i,j}} C(x, y, t), dx, dy$, where $|g_{i,j}|$ denotes the cell area. This gridding process creates a discrete representation while preserving the spatial distribution characteristics of the oil spill. The temporal evolution of the oil spill is captured through a sequence of grid states $G_{t\,t=0}^{T}$ at discrete time steps.

B. Uncertainty Modeling Based on Information Entropy

Oil spill dynamics are characterized by temporal changes in concentration patterns. For each grid cell, we define the change rate between consecutive time steps as the absolute difference $\Delta c_{i,j}(t) = |c_{i,j}(t) - c_{i,j}(t-1)|$. To further quantify the uncertainty associated with these temporal changes, we compute the average change rate over a sequence of k recent time steps:

$$\bar{\Delta} c_{i,j} = \frac{1}{k-1} \sum_{t=2}^{k} |c_{i,j}(t) - c_{i,j}(t-1)|. \tag{1}$$

This average change rate serves as the baseline for uncertainty, indicating regions with rapid spill evolution that require more frequent monitoring. A minimum uncertainty u_{min} is added for all grid cells: $u_{i,j} = u_{min} + \bar{\Delta} c_{i,j}$. The uncertainty values are then mapped to information entropy using a binary entropy model, where $p = 0.5 \cdot u_{i,j}$:

$$H(u_{i,j}) = -p \log_2 p - (1-p) \log_2 (1-p). \tag{2}$$

The aforementioned entropy model quantifies the information uncertainty of oil spill regions by capturing temporal variations in oil concentration. These variations are then mapped to entropy values for each grid cell. Fig. 2. presents a representative entropy map, where regions with higher entropy indicate greater uncertainty and demand prioritized monitoring.

C. Drift Information Freshness

In practical persistent monitoring, the timeliness of the acquired dynamic oil spill region information, which is referred to as DIF, plays a critical role. DIF reflects the extent to which the most recently collected data at each grid cell accurately represents the current state of the environment. If a high-entropy region is not revisited promptly, the value of its observed information degrades rapidly, diminishing the effectiveness of the monitoring mission. In contrast, low-entropy regions can tolerate longer intervals between observations without a marked drop in information freshness.

To address this, we define a polynomial-decay weighted information freshness metric that accounts for both the monitoring priority and the timeliness of each grid cell. Specifically, the information freshness for the monitored region is formulated as:

$$F_{\text{region}}^{*} = \frac{\sum_{g \in \text{region}} w(g) \left[\frac{1}{1+\lambda E(g) \cdot s(g)} \right]}{\sum_{g \in \text{region}} w(g)} \tag{3}$$

where $E(g)$ denotes the entropy value of grid cell g, $s(g)$ is the visiting step at which g was observed (with unvisited cells set to zero), and λ is a decay parameter. The weight $w(g)$ is typically set as $E(g)^{\alpha}$ to emphasize the contribution of high-entropy cells, where α controls the degree of emphasis. This metric highlights the monitoring value of quickly visiting high-uncertainty regions, as timely revisits to these uncertain regions are essential for maintaining up-to-date environmental awareness.

D. Multi-UAV Oil Spill Monitoring Problem Formalization

A periodic monitoring strategy is adopted, in which multiple UAVs are allocated to dynamic oil spill regions in proportion to their area. During each monitoring cycle, UAVs are dispatched to the newly emerged regions to collect up-to-date information on spill dynamics. When the area of newly identified regions continuously decreases over several cycles, which indicates that the oil spill region has stabilized, the UAV monitoring process is terminated. The monitoring performance is evaluated by three core metrics: coverage rate, total flight distance, and drift information freshness (DIF). The coverage rate reflects the overall thoroughness of monitoring. The total flight distance represents the number of grid cells traversed by UAVs, with jump distances calculated using the Manhattan distance. The DIF quantifies the timeliness of the oil spill data acquired during the current cycle.

- **Coverage Rate:** The proportion of the target oil spill region that has been effectively observed during a monitoring cycle, calculated as

$$\text{Coverage Rate} = \frac{\sum_{g \in S_t} O_t(g)}{\sum_{g \in S_t} 1} \tag{4}$$

  where S_t denotes the set of target grid cells and $O_t(g)$ indicates whether cell g has been observed (1 if observed, 0 otherwise).
- **Total Flight Distance:** The total distance traveled by all UAVs during the current monitoring cycle. It is computed as the sum of the path lengths of all UAVs within that cycle:

$$D_{\text{step}}(t) = \sum_{k=1}^{N} \sum_{i=1}^{n_k^{(t)}-1} d\left(p_i^{k,(t)}, p_{i+1}^{k,(t)}\right) \tag{5}$$

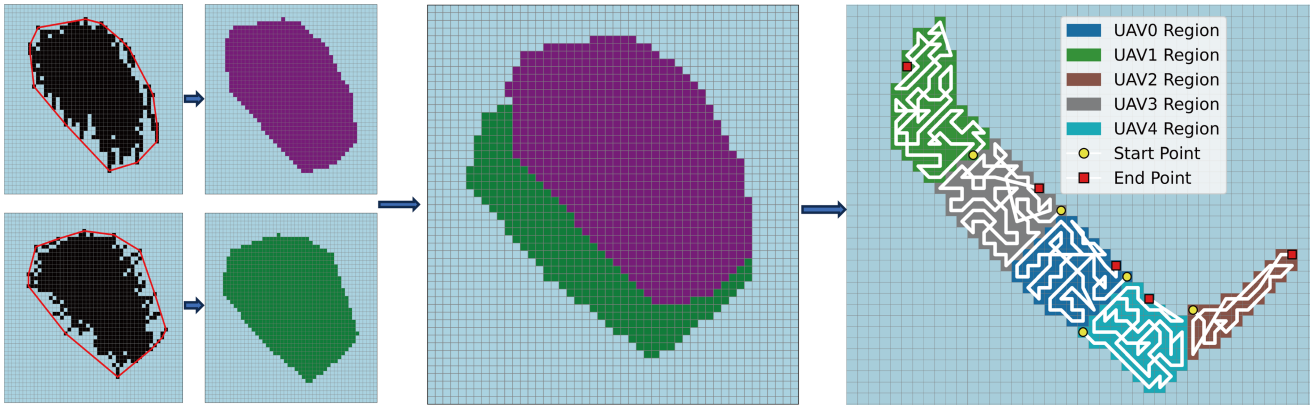

Fig. 3. Illustration of the incremental region extraction process. The left column illustrates the oil spill grids (black) along with their convex hulls (red line) for two consecutive monitoring cycles. The middle column presents the convex hull regions for the previous cycle (purple) and the current cycle (green), where the overlapping and incremental regions are visually distinguished. The right column shows the region division and path planning for the incremental area.

where t denotes the monitoring cycle, N is the number of UAVs, $n_k^{(t)}$ is the number of waypoints for UAV k in cycle t, and $d(p_i^{k,(t)}, p_{i+1}^{k,(t)})$ represents the distance between consecutive waypoints along the path of UAV k in cycle t.

- **Drift Information Freshness:** The timeliness of acquired monitoring data, with greater emphasis on high-uncertainty areas. The specific definition is given in (3).

Under the premise of ensuring sufficient CR, our objective is to maximize the DIF value, while also reducing UAV flight distance. Formally, the optimization problem can be expressed as:

$$
\begin{aligned}
[1em][l]\max \quad & \mathrm{DIF}(P_1, \ldots, P_N) \\
[1em][l]\min \quad & D_{\text{total}} = \sum_{k=1}^{N} \sum_{i=1}^{n_k-1} d(p_i^k, p_{i+1}^k) \\
[1em][l]\text{s.t.} \quad & \mathrm{CR}(P_1, \ldots, P_N) \geq \theta, \\
& \sum_{i=1}^{n_k-1} d(p_i^k, p_{i+1}^k) \leq L_{\max}, \quad \forall k \in \{1, \ldots, N\}.
\end{aligned} \tag{6}
$$

III. Multi-UAV Monitoring Framework

Our proposed multi-UAV monitoring framework is structured around three core components: (i) an incremental coverage path planning mechanism, (ii) region division, and (iii) an entropy-based path planning algorithm.

The incremental coverage mechanism identifies newly emerged oil spill regions at each monitoring cycle and focuses UAV resources on these areas, thereby reducing redundant monitoring and improving overall efficiency. The entropy-based region division algorithm ensures balanced and information-driven allocation of monitoring tasks by partitioning the incremental region into subregions according to both spatial distribution and local information entropy. The coverage path planning algorithm then generates efficient coverage paths for each UAV, explicitly considering both DIF and the practical endurance limits of the UAVs, including jump strategies for highly discrete or fragmented spill regions.This process is illustrated in Fig. 3.

A. Incremental Coverage Path Planning Mechanism

To avoid redundant monitoring and efficiently allocate UAV resources, we adopt an incremental coverage path planning mechanism that focuses exclusively on newly emerged oil spill regions. The core idea is to identify and decompose new oil-affected areas at each monitoring cycle, and subsequently plan UAV coverage paths tailored to these incremental regions.

Let S_t denote the set of oil spill grid cells detected in the current monitoring round, and S_{t-1} the set from the previous cycle. The new region R_{new} to be covered is defined as the difference between the current and previous spill regions, i.e., $R_{\text{new}} = S_t \setminus S_{t-1}$. Given the irregular and dynamic nature of oil spills, we represent S_t and S_{t-1} using their convex hulls, denoted as CH_t and CH_{t-1}. The incremental region is computed as the set of grid cells lying inside CH_t but outside CH_{t-1}. For a grid map of size $M \times N$, the new region is determined by $R_{\text{new}} = \{(x, y) \mid (x, y) \in CH_t,\ (x, y) \notin CH_{t-1}\}$, where (x, y) are the coordinates of the grid cell center.

B. Region Division

After extracting the incremental region, we design a balanced partitioning approach to assign monitoring subregions to UAVs. The proposed entropy-weighted region division algorithm distributes the monitoring workload while considering both the spatial distribution and the relative uncertainty of newly emerged oil spill areas.

Given the set of points $P = (x_i, y_i)$ in the new region and the corresponding entropy map $E(x, y)$, the algorithm first computes an entropy-based weight for each point as $w_i = E(x_i, y_i) + \epsilon$, where ϵ is a small constant to avoid zero weights. Partitioning is then initialized using weighted K-means clustering, in which points with higher entropy values are replicated more frequently and therefore gain greater influence in the

IEEE Robotics and Automation Letters (RA-L) paper, presented at ICRA 2026, Vienna, Austria. Cite as RA-L paper.

clustering process. This results in n initial clusters, where n is the number of UAVs.

However, K-means clustering itself suffers from two limitations. First, it does not guarantee workload balance, which may result in significant disparities among cluster sizes and even cause individual UAV workloads to exceed endurance limits. To address this, we minimize the variance of cluster sizes under the endurance constraint $|C_k| \leq C_{\max},\ \forall k$, where $|C_k|$ denotes the number of cells in cluster C_k and $C_{\max}$ is the maximum effective coverage capacity of a single UAV. Second, K-means does not ensure spatial connectivity within clusters; in irregular spill regions, this may cause a UAV to be assigned to disjoint sub-areas, which is impractical in real operations. To resolve this, each cluster is required to form a connected component in the adjacency graph G, expressed as $C_k \subseteq G$ is connected, $\forall k$.

In practice, these constraints are satisfied through lightweight adjustments, including redistributing points between overloaded and underloaded clusters, repairing connectivity by bridging disconnected fragments or reallocating isolated points, and merging undersized clusters ($|C_k| < \tau$, with $\tau = 8$ in our implementation) into nearby larger ones. This ensures that each UAV is eventually assigned a spatially continuous and endurance-feasible monitoring region while preserving the computational efficiency of k-means.

Before region division, it is also necessary to estimate the required number of UAVs, i.e., to determine the number of subregions to be partitioned, so as to ensure that the endurance of each UAV is sufficient to cover its assigned subregion. Specifically, the estimation is based on the approximate size of the new region $|R_{\text{new}}|$, and then combined with the maximum flight distance of a single UAV, R_{flight}. To account for operational uncertainties, only 80% of the maximum flight distance is considered, and a path efficiency factor α is introduced to define the effective coverage capacity of a single UAV. The required number of UAVs is equal to the number of subregions to be partitioned, and it is calculated as:

$$N_{\text{drones}} = N_{\text{subregions}} = \max\left(1,\ \left\lceil \frac{|R_{\text{new}}| \cdot \eta}{\alpha \cdot R_{\text{flight}}} \right\rceil\right), \qquad (7)$$

where $\eta = 0.9$ denotes the target coverage rate, and α is the path efficiency factor. This estimation guarantees that the assigned UAV team has sufficient endurance to cover the new region, thereby preventing incomplete monitoring due to insufficient flight range.

C. Entropy-Based Path Planning

Coverage path planning over newly emerged oil spill regions is challenging, as the spatial distribution of oil is often highly discrete, fragmented, or disconnected. If the planner only allows stepwise movement to directly adjacent cells, certain isolated or remote grid cells may remain unreachable, which compromises the overall coverage rate and information gain.

To address this issue, we first represent all newly emerged oil spill grids as nodes in an undirected weighted graph G, where each node corresponds to a candidate coverage cell and is assigned an entropy value reflecting its monitoring priority.

Algorithm 1: Entropy-Based Path Planning.

Input: G, p_s, E, $d_{\max}$, $d_{\text{jump,max}}$; **Output:** P
Initialize $P = [p_s]$, $visited = \{p_s\}$, $current = p_s$, $distance = 0$
while $|visited| < |V|$ **and** $distance < d_{\max}$ **do**
  $adj\_candidates \leftarrow$ unvisited neighbors of $current$
  if $adj\_candidates \neq \emptyset$ **then**
    $H(n) = E(n) \times bonus$, $next = \arg\max H(n)$, $step\_dist = 1$
  else
    $jump\_candidates \leftarrow$ unvisited nodes within $d_{\text{jump,max}}$ and budget
    if $jump\_candidates = \emptyset$ **then**
      break
    end if
    $H(n) = E(n)/(1 + \lambda d(current, n))$, $next = \arg\max H(n)$, $step\_dist = d(current, next)$
  end if
  if $distance + step\_dist > d_{\max}$ **then**
    break
  end if
  Append $next$ to P, mark visited; update $current, next, distance$
end while

Edges are established between neighboring nodes based on an 8-connectivity rule, and the edge weights are defined inversely proportional to the sum of the entropy values of the connected nodes, so that high-entropy regions are more likely to be prioritized during path planning.

Building upon this entropy-weighted graph, we introduce a *jump* mechanism into our path planning. Specifically, when necessary, the UAV is allowed to move directly from the current cell to a non-adjacent node within a reasonable distance in G, enabling coverage of spatially isolated or fragmented regions that cannot be reached by local moves alone.

However, frequent or long-range jumps may lead to increased UAV energy consumption and decreased path efficiency. Therefore, our method allows jumping while imposing two practical constraints:

- **Maximum single-step jump distance constraint**: Each jump must not exceed a predefined threshold $d_{\text{jump,max}}$, preventing the UAV from making energy-intensive or impractically long transitions.
- **Remaining endurance constraint**: Regardless of whether the step is local or a jump, the actual travel distance for each step must not exceed the UAV's remaining flight range, ensuring that the entire path stays within the UAV's endurance budget.

Within this framework, the path planning process proceeds as follows: at each step, the algorithm gives priority to unvisited adjacent nodes in G with high entropy values. When all neighboring points have been visited or cannot be reached within the remaining range, the algorithm considers jumping to a more

IEEE Robotics and Automation Letters (RA-L) paper, presented at ICRA 2026, Vienna, Austria. Cite as RA-L paper.

TABLE I
SIMULATION

Scenario	Spill scale	Initial spill area (km^2)	Grid map size
1	Small	20	60×60
2	Medium	80	80×80
3	Large	300	100×100

TABLE II
REAL-WORLD EXPERIMENT

Scenario	Start Time (UTC)	Location	Source
4	2021-05-01 09:56	36°04'N, 120°14'E	Sen-1, GF-1
5	2018-01-18 02:20	28°22'N, 125°55'E	Sen-2
6	2010-04-25 13:00	28°44'N, 88°23'W	ALOS

distant, unvisited node that satisfies both the jump distance and endurance constraints and offers the highest expected entropy gain.

To further optimize path selection, a heuristic function is incorporated: adjacent points are rewarded to boost their selection priority, while distant jump candidates are penalized by their distance, encouraging the UAV to prefer local, continuous movement and jump only when necessary. The heuristic score $H(n)$ for a candidate node n is defined as follows:

$$H(n) = \begin{cases} & \text{if n is adjacent to} \\ E(n) \cdot \alpha, & \text{the current node} \\ [2pt] \frac{E(n)}{1+\lambda \cdot d(\text{current},n)}, & \text{if n is a jump candidate} \end{cases} \tag{8}$$

The overall procedure of the proposed entropy-based path planning algorithm is summarized in Algorithm 1.

IV. EXPERIMENTS

In this section, the proposed framework is evaluated in both simulation and real-world oil spill data. Our experiments aim to justify the following content:

1) We demonstrated the robustness and scalability of the proposed method (EICPP) through three simulated oil spill scenarios of different scales and three real oil spill scenarios.

2) We validated the effectiveness of the proposed entropy-based method by comparing it with three baseline algorithms, DARP-ε, Vor-A$*$, and MSTC$*$, using DIF and TFD as evaluation metrics.

3) Through two ablation studies, namely comparisons with the NE and NIM algorithms, we validated the effectiveness of the incremental coverage mechanism and the entropy-based path planning strategy.

A. Experimental Setup

We generated three simulated oil-spill scenarios of different scales using OpenDrift, with configuration details summarized in Table I. In addition, we obtained the real oil spill data of the *Symphony* oil spill accident (Scenario4), the *Sanchi* tanker oil spill accident (Scenario5), and the *Deepwater Horizon* oil spill accident (Scenario6) from [11], [12]. Based on these datasets, we conducted experiments on real-world oil spill scenarios, with key parameters summarized in Table II. The maximum single-flight range of each UAV is set to 27 km, which corresponds to a flight distance of 45 grid cells. The information freshness decay factor λ_{decay} is 0.1. In the weighted K-means region division, the maximum iterations is 10, and the tolerance is $\max(1, \lfloor \text{target\_size}/3 \rfloor)$, where target_size is the average number of grid cells per UAV. In entropy-guided path planning, the maximum jump distance is 10 to avoid large jumps between disconnected subregions. The current monitoring strategy is to conduct detection every two hours and return the collected data after each round.

The proposed multi-UAV monitoring framework is evaluated across the six representative oil spill scenarios, using three performance metrics: Coverage Rate (CR), Total Flight Distance (TFD), and Drift Information Freshness (DIF). Our optimization objective is to maximize the DIF and minimize the TFD, while ensuring that a designated 90% CR is achieved.

For each scenario, we compare our approach **(EICPP)** with five baseline methods:

- **No Incremental Mechanism method (NIM):** UAVs monitor the entire oil spill region in every monitoring round, without distinguishing newly emerged areas from previously covered ones.
- **No Entropy-based method (NE):** UAVs perform uniform coverage in each round, without considering entropy information or prioritizing high-uncertainty areas.
- **DARP-ε^*-coverage method (DARP-ε^*):** An extension of greedy coverage strategies that integrates A$*$ search, DARP-based region partitioning, and ε^*-guided adjustments to improve path efficiency and adaptability.
- **Voronoi-based-A$*$-coverage method (Vor-A$*$):**A coverage method that partitions the oil spill region into Voronoi cells and plans paths within each cell using the A$*$ search algorithm, focusing on efficient local path generation under information-guided constraints.
- **Multi-robot Spanning Tree Coverage method (MSTC$*$):**A coverage method that constructs a spanning tree over the discretized oil spill region and assigns branches to multiple UAVs for systematic and efficient coverage.

B. Performance Analysis

Through evaluations conducted under three simulated scenarios and three real oil spill scenarios, and by comparison with five baseline algorithms, the proposed oil spill monitoring framework was demonstrated to be both robust and scalable, highlighting the advantages of the proposed method. The ablation studies further validated the effectiveness of its core components.

The DIF values of each monitoring round compared with the baseline methods are illustrated in Figs. 4 and 5. The Average DIF (Avg.DIF) results are summarized in Table III, while the Average Total Flight Distance (Avg.TFD) comparison is presented in Table IV.

In the small-, medium-, and large-scale spill scenarios (Scenarios 1–3), EICPP consistently outperforms the five baseline methods in terms of average DIF (Avg.DIF) (Table III). In the small-scale spill scenario (Scenario 1), EICPP achieves an

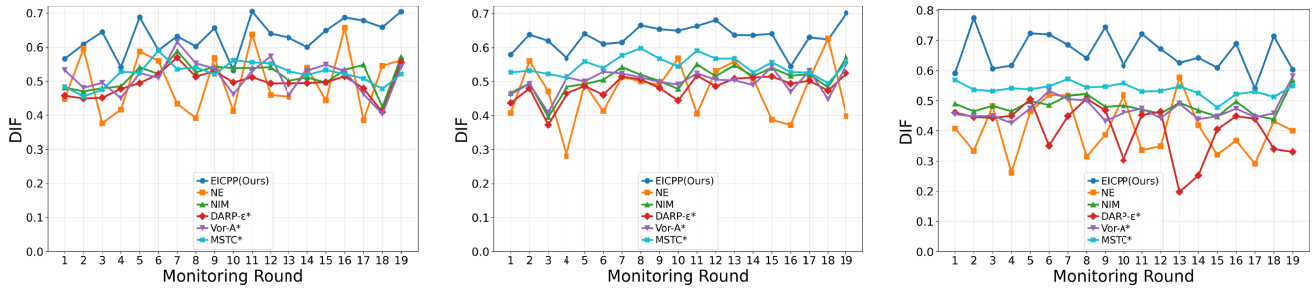

(a) Scenario 1: Small, $20\,\mathrm{km}^2$, 60×60 (b) Scenario 2: Medium, $80\,\mathrm{km}^2$, 80×80 (c) Scenario 3: Large, $300\,\mathrm{km}^2$, 100×100

Fig. 4. Drift Information Freshness (DIF) for Scenarios 1–3. All results are obtained under the requirement of achieving at least 90% coverage.

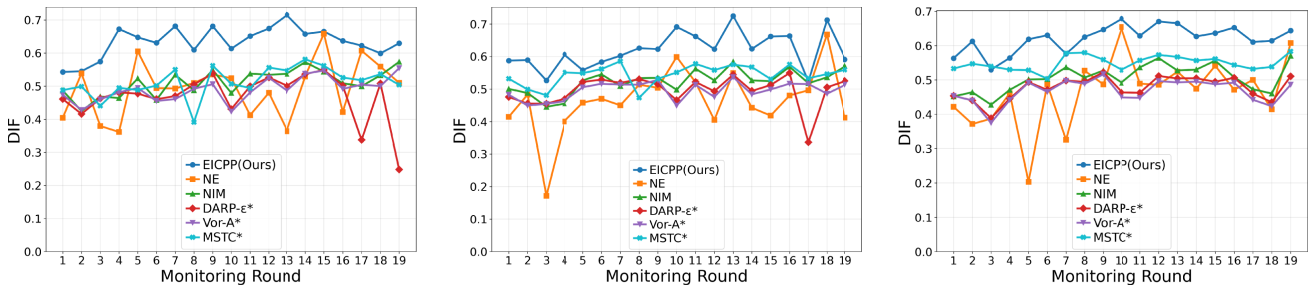

(a) Scenario 4: Symphony spill (b) Scenario 5: Sanchi spill (c) Scenario 6: Deepwater Horizon spill

Fig. 5. Drift Information Freshness (DIF) for Scenarios 4–6. All results are obtained under the requirement of achieving at least 90% coverage.

TABLE III
AVERAGE DIF COMPARISON ACROSS SIX SCENARIOS (UNIT: GRID CELLS)

Scenario	**EICPP**	NE	NIM	DARP-ε*	Vor-A*	MSTC*
1	**0.63**	0.49	0.51	0.49	0.51	0.52
2	**0.64**	0.47	0.50	0.48	0.49	0.54
3	**0.65**	0.40	0.48	0.40	0.46	0.53
4	**0.63**	0.49	0.51	0.46	0.49	0.51
5	**0.61**	0.46	0.52	0.49	0.49	0.51
6	**0.62**	0.46	0.50	0.47	0.46	0.50

TABLE IV
AVERAGE TFD COMPARISON ACROSS SIX SCENARIOS (UNIT: GRID CELLS)

Scenario	**EICPP**	NE	NIM	DARP-ε*	Vor-A*	MSTC*
1	**197**	210	823	965	870	867
2	**320**	340	1811	2134	1909	1883
3	**455**	460	2713	3261	2943	2905
4	**208**	219	928	1090	1092	963
5	**352**	360	1678	1992	1982	1764
6	**448**	501	2138	2517	2509	2227

improvement of about 20% compared with the strongest baseline MSTC$*$, and an improvement of up to 60% compared with the weakest baseline NE, demonstrating consistent advantages across different levels of baseline algorithms. As the spill scale increases (Scenarios 2–3), EICPP maintains stable performance gains, achieving 18–25% Avg.DIF improvement over strong baselines, which indicates its ability to ensure Avg.DIF even under higher coverage complexity. Meanwhile, the results of Avg.TFD show that EICPP significantly reduces the flight burden of UAVs. With the expansion of spill scale, the advantages of the incremental coverage mechanism become more evident. For example, in Scenario 3, the TFD of EICPP is only 455, whereas MSTC$*$, DARP-ε^*, and Voronoi-A$*$ all exceed 2900, thus greatly improving path efficiency and avoiding large-scale redundant coverage.

In the *Symphony* spill case (Scenario 4), EICPP achieves an Avg.DIF of 0.63 compared with 0.51 for MSTC$*$, corresponding to a relative improvement of about 23.5%. This indicates that the proposed method is able to sustain higher information freshness even in medium-scale real spill scenarios with irregular morphology. In the *Sanchi* tanker spill case (Scenario 5), EICPP records an Avg.DIF of 0.61, which is approximately 19.6% higher than MSTC$*$ (0.51), and 24.5% higher than DARP-ε^* (0.49). These comparisons further confirm that the advantage in information freshness is consistently maintained under varying spill scales and complexities. When combined with the results from simulated scenarios (Scenarios 1–3), where improvements over strong baselines remain within 18–25%, the framework demonstrates consistent performance across both synthetic and real-world conditions.

At the same time, EICPP continues to demonstrate substantial savings in TFD, thereby improving monitoring efficiency and

IEEE Robotics and Automation Letters (RA-L) paper, presented at ICRA 2026, Vienna, Austria. Cite as RA-L paper.

reducing resource consumption. For instance, in the *Deepwater Horizon* accident (Scenario 6), which represents one of the most challenging and large-scale oil spill disasters, the TFD of EICPP is only 448, while MSTC$*$ and DARP-ε^* reach 2227 and 2517, respectively. These results indicate that EICPP not only improves Avg.DIF but also effectively reduces the flight burden, reflecting the intended advantages of the incremental coverage mechanism.

Through two ablation studies, namely comparisons with the NE and NIM algorithms, the effectiveness of the incremental coverage mechanism and the entropy-based path planning strategy was validated. As shown in Tables III and IV, EICPP was consistently found to outperform both NE and NIM across all six scenarios in terms of both Avg.DIF and TFD. For instance, in Scenario 3, an Avg.DIF of 0.65 was achieved by EICPP compared to 0.40 (NE) and 0.48 (NIM), while the TFD was simultaneously reduced from 2713 (NIM) to only 455. Similar trends were observed in other scenarios, where higher information freshness was achieved alongside substantial reductions in flight distance.

The computational complexity of the EICPP framework is analyzed to verify its scalability and real-time feasibility. The main operations include entropy map update, weighted K-means clustering, and entropy-guided path planning, with complexities of $O(N)$, $O(NKI)$, and $O(N \log N)$, respectively. Thus, the overall complexity per re-planning window is $O(NKI + N \log N)$, and parallel path construction allows near-linear growth with N.

V. Conclusion

In summary, this letter presents an entropy-based incremental multi-UAV monitoring framework for efficient coverage of dynamic oil spill regions. By combining uncertainty quantification, an incremental coverage mechanism, and entropy-based path planning, the proposed method enables UAVs to prioritize high-entropy areas while avoiding redundant coverage. Experimental evaluations show that the framework consistently improves DIF and reduces TFD, validating its effectiveness. Our method achieves 19–25% improvement in DIF over strong baselines across various spill scales, with a 19.6–24% improvement on real-world oil spill datasets. It also significantly reduces flight distance while ensuring 90% coverage.

Moreover, we emphasize the significance of Avg.DIF. While traditional metrics such Coverage Rate and TFD can reflect monitoring efficiency, they are insufficient to fully capture the practical value of monitoring in rapidly evolving spill scenarios. In contrast, Avg.DIF directly quantifies the timeliness and utility of monitoring data, reflecting the urgency of information acquisition and its contribution to emergency response.

Future work will explore the integration of sensing uncertainty, UAV failures, and communication constraints to further enhance applicability. In addition, potential applications and extensions in large-scale oil spill emergency monitoring tasks will be investigated. Moreover, we plan to integrate battery-aware cost terms into the path-planning process and enable real-time role switching among UAVs based on their remaining energy levels to enhance long-term sustainability.

References

[1] C. P. Brussaard et al., "Immediate ecotoxicological effects of short-lived oil spills on marine biota," *Nature Commun.*, vol. 7, no. 1, 2016, Art. no. 11206.

[2] S. B. Joye, "Deepwater horizon, 5 years on," *Science*, vol. 349, no. 6248, pp. 592–593, 2015.

[3] S. K. Chaturvedi, S. Banerjee, and S. Lele, "An assessment of oil spill detection using sentinel 1 SAR-C images," *J. Ocean Eng. Sci.*, vol. 5, no. 2, pp. 116–135, 2020.

[4] S. Mohammadiun, G. Hu, A. A. Gharahbagh, J. Li, K. Hewage, and R. Sadiq, "Intelligent computational techniques in marine oil spill management: A critical review," *J. Hazardous Mater.*, vol. 419, 2021, Art. no. 126425.

[5] Z. Wei et al., "UAV-assisted data collection for Internet of Things: A survey," *IEEE Internet Things J.*, vol. 9, no. 17, pp. 15460–15483, Sep. 2022.

[6] Z. Yang et al., "UAV remote sensing applications in marine monitoring: Knowledge visualization and review," *Sci. Total Environ.*, vol. 838, 2022, Art. no. 155939.

[7] A.-L. Balogun, S. T. Yekeen, B. Pradhan, and K. B. W. Yusof, "Oil spill trajectory modelling and environmental vulnerability mapping using GNOME model and GIS," *Environ. Pollut.*, vol. 268, 2021, Art. no. 115812.

[8] E. Galceran and M. Carreras, "A survey on coverage path planning for robotics," *Robot. Auton. Syst.*, vol. 61, no. 12, pp. 1258–1276, 2013.

[9] D. Datsko, F. Nekovar, R. Penicka, and M. Saska, "Energy-aware multi-UAV coverage mission planning with optimal speed of flight," *IEEE Robot. Autom. Lett.*, vol. 9, no. 3, pp. 2893–2900, Mar. 2024.

[10] K. Shah, G. Ballard, A. Schmidt, and M. Schwager, "Multidrone aerial surveys of penguin colonies in antarctica," *Sci. Robot.*, vol. 5, no. 47, 2020, Art. no. eabc3000.

[11] P. Ren et al., "Oil spill drift prediction enhanced by correcting numerically forecasted sea surface dynamic fields with adversarial temporal convolutional networks," *IEEE Trans. Geosci. Remote Sens.*, vol. 63, 2025, Art. no. 4701018.

[12] Q. Zhu et al., "Oil spill contextual and boundary-supervised detection network based on marine SAR images," *IEEE Trans. Geosci. Remote Sens.*, vol. 60, 2022, Art. no. 5213910.

[13] L. Feng and J. Katupitiya, "UAV-based persistent full area coverage with dynamic priorities," *Robot. Auton. Syst.*, vol. 157, 2022, Art. no. 104244.

[14] M. d. O. Soares, C. Teixeira, L. Bezerra, S. Rossi, T. Tavares, and R. Cavalcante, "Brazil oil spill response: Time for coordination," *Science*, vol. 367, no. 6474, pp. 155–155, 2020.

[15] X. Ye et al., "A multi-criteria simulation-optimization coupling approach for effective emergency response in marine oil spill accidents," *J. Hazardous Mater.*, vol. 469, 2024, Art. no. 133832.

[16] R. Pagnucco and M. L. Phillips, "Comparative effectiveness of natural by-products and synthetic sorbents in oil spill booms," *J. Environ. Manage.*, vol. 225, pp. 10–16, 2018.

[17] O. Alvear, N. R. Zema, E. Natalizio, and C. T. Calafate, "Using UAV-based systems to monitor air pollution in areas with poor accessibility," *J. Adv. Transp.*, vol. 2017, no. 1, 2017, Art. no. 8204353.

[18] O. M. Bushnaq, A. Chaaban, and T. Y. Al-Naffouri, "The role of UAV-IoT networks in future wildfire detection," *IEEE Internet Things J.*, vol. 8, no. 23, pp. 16984–16999, Dec. 2021.

[19] Q. Guo, W. Xu, J. Peng, H. Li, and Z. Xiang, "Persistent monitoring for points of interests with different priorities using multiple UAVs," in *Proc. IEEE 28th Int. Conf. Parallel Distrib. Syst.*, 2023, pp. 427–434.

[20] T. M. Cabreira, L. B. Brisolara, and F. J. Paulo R, "Survey on coverage path planning with unmanned aerial vehicles," *Drones*, vol. 3, no. 1, 2019, Art. no. 4.

[21] J. Tang, C. Sun, and X. Zhang, "MSTC: Multi-robot coverage path planning under physical constrain," in *Proc. IEEE Int. Conf. Robot. Automat.*, 2021, pp. 2518–2524.

[22] G. Sanna, S. Godio, and G. Guglieri, "Neural network based algorithm for multi-UAV coverage path planning," in *Proc. Int. Conf. Unmanned Aircr. Syst.*, 2021, pp. 1210–1217.

[23] T. M. Cabreira, C. Di Franco, P. R. Ferreira, and G. C. Buttazzo, "Energy-aware spiral coverage path planning for UAV photogrammetric applications," *IEEE Robot. Autom. Lett.*, vol. 3, no. 4, pp. 3662–3668, Oct. 2018.

[24] J.-M. Lien, S. Rodriguez, and M. Morales, "Persistent covering with latency and energy constraints," *IEEE Robot. Autom. Lett.*, vol. 6, no. 2, pp. 998–1003, Apr. 2021.

[25] K.-F. Dagestad, J. Röhrs, Ø. Breivik, and B. Ådlandsvik, "Opendrift V1. 0: A generic framework for trajectory modelling," *Geoscientific Model Develop.*, vol. 11, no. 4, pp. 1405–1420, 2018.